

Domain Structure and Conformational Changes in rat Kv2.1 ion Channel

Anastasia Grizel · Anna Popinako ·
Marina A. Kasimova · Louisa Stevens · Maria Karlova ·
Mikhail M. Moisenovich · Olga S. Sokolova

Received: 13 March 2014 / Accepted: 3 September 2014
© Springer Science+Business Media New York 2014

Abstract Voltage-gated potassium Kv2.1 channels are widely distributed in the central nervous system, specifically in neuroendocrine and endocrine cells. Their cytoplasmic C-termini are large and carry out many important functions. Here we provide the first direct structural evidence that each C-terminal part within the Kv2.1 ion channel is formed by two distinct domains (Kv2 and CTA). We expressed and purified two C-terminal truncation mutants of a rat Kv2.1 channel, lacking the entire C-termini or the CTA domain. Single particle electron microscopy was used to obtain three-dimensional reconstructions of purified C-terminal Kv2.1 mutants at 2.0 and 2.4 nm resolution. Comparison of these structures to each other and to the low-resolution EM structure of the full-length Kv2.1 channel revealed the exact locations of cytoplasmic Kv2 and CTA domains within the tetramer. Four Kv2 domains envelop the N-terminal T1 domain. The tetramer of the CTA

domains underlies the Kv2-T1 complex and may also affect the channel's surface expression. Subsequent molecular dynamics simulation and homology modeling produced open and closed structural models of the membrane part of the Kv2.1 channel.

Keywords Kv2 channel · Single particle electron microscopy · Cytoplasmic domains · Kv2 · CTA · Molecular homology modeling · Conformational changes

Abbreviations

Kv	Voltage-gated potassium channel
AgTx2	Agitoxin2
EM	Electron microscopy
3D	Three-dimensional
CTF	Contrast transfer function
FSC	Fourier shell correlation
MRA	Multi-reference analysis
MSA	Multivariate statistical analysis
MD	Molecular dynamics
RMSD	Root mean square deviation
VSD	Voltage-sensor domain

Electronic supplementary material The online version of this article (doi:10.1007/s11481-014-9565-x) contains supplementary material, which is available to authorized users.

A. Grizel
Saint Petersburg State University, Saint Petersburg 199034, Russia

A. Popinako
N.A.Bakh Institute of Biochemistry RAS, Moscow 119071, Russia

M. A. Kasimova · M. Karlova · M. M. Moisenovich ·
O. S. Sokolova (✉)
Faculty of Biology, M.V. Lomonosov Moscow University, 1
Leninskie Gory, Bld.12, 119991 Moscow, Russia
e-mail: sokolova184@gmail.com

L. Stevens
Institute of Membrane and Systems Biology, Leeds University,
Leeds LS2 9JT, UK

O. S. Sokolova
A.V. Shubnikov Institute of crystallography RAS, Moscow 119333,
Russia

Introduction

Voltage-gated potassium (Kv) channels play a critical role in cell function providing a membrane potential and repolarization of the action potential (Pongs 2009). Kv channels represent a very diverse group that subdivides into 12 subfamilies: Kv1 – Kv12 (Gutman et al. 2005; Pischalnikova and Sokolova 2009). Among them, Kv2 are the prevalent channels within the central nervous system, neuroendocrine and endocrine cells, such as pancreatic B-cells (Murakoshi and Trimmer 1999; Antonucci et al. 2001; Malin and Nerbonne 2002).

The knockout of Kv2.1 in isolated islets enhances insulin secretion and may result in the development of type 2 diabetes (MacDonald et al. 2001). The overexpression of Kv2.1 channels has been reported in cervical adenocarcinoma cells (Suzuki and Takimoto 2004).

Similar to other Kv channels, Kv2.1 are tetramers with each monomer consisting of six transmembrane segments S1 to S6. The membrane-embedded domain accommodates a voltage-sensing domain (VSD) and an ion-selective pore (segments S5-S6). The amino and carboxyl termini of the channel are situated in the cytoplasm. Within the N-terminal intracellular region (180 residues) there is a characteristic feature for the majority of Kv channels, the T1 domain (residues 28–139) (Papazian 1999). The crystal structure of the T1 domain was first obtained for the *Shaker* channel (Kreusch et al. 1998). The T1 domain is responsible for tetramerization and interacts with auxiliary subunits that assist in the regulation of important channel functions, such as surface localization and intracellular trafficking (Gulbis et al. 2000; Kim et al. 2004). Existing biochemical data suggests that Kv2.1 channels are lacking the cytoplasmic auxiliary subunits (Chung and Li 2005). In cells, the Kv2.1 channels form high-density clusters within the plasma membrane (Trimmer 1991; Antonucci et al. 2001; Tamkun et al. 2007), and the endoplasmic reticulum of somatic and proximal dendrites of pyramidal neurons (Du et al. 1998). Clusters are thought to associate with a distinct group of Ca²⁺ signaling proteins (Antonucci et al. 2001) and with the cortical actin cytoskeleton (Tamkun et al. 2007) through the C-termini of Kv channels (Mohapatra et al. 2008). The C-termini of Kv2.1 are rather large (50 % of the amino acids are located in the C-termini) and are thought to comprise at least two major domains: the Kv2 domain (~250 amino acids) and the C-terminal activation or CTA domain (~112 amino acids) (Ju et al. 2003; Wray 2004, 2009). The CTA domain is involved in the determination of channel activation (Ju et al. 2003; Wray 2004).

Despite its undeniable importance, the atomic structure of the Kv2.1 channel is currently unavailable. Single particle EM of the full length Kv2.1 channel revealed the overall 3D structure of the whole molecule at the 25 Å resolution (Adair et al. 2008), but its exact 3D architecture remains unknown. The large density observed beneath the membrane-embedded domain is thought to be the C-terminal domains, which may interact with each other (VanDongen et al. 1990; Ju et al. 2003; Wray 2009) and with the N-terminal T1 domain (Kobrinsky et al. 2006; Mohapatra et al. 2008). But there were no direct structural data on the localization of C- and N-termini with respect to one another.

Here we studied the structure of the Kv2.1 ion channel using single particle EM and molecular dynamics simulation. We provide direct structural evidence that the C-termini of the Kv2.1 ion channel are formed by two distinct domains (Kv2 and CTA) that surround the N-terminal T1 tetramer.

Methods

All chemicals, unless otherwise specified, were purchased from Sigma. The Metafecten™ PRO kit was purchased from Biointex (Germany). 1D4 antibodies were purchased from the National Cell Culture Center (Minneapolis, USA), and the 1D4 elution peptide was purchased from American Peptide (Sunnyvale, CA). Cy3 fluorescent dye was purchased from FLUMAN (Russia). Protease inhibitor tablets were purchased from Pierce. The expression pCSP105 vector containing the fusion construct of Agitoxin 2 (AgTx2) was generously donated by Professor C. Miller (Brandeis University, Waltham, MA).

Generation of Kv2.1 Mutants Kv2.1-pMT3 wild type was constructed by inserting Kv2.1 between residues 2 and 853, using the standard PCR overlap extension method (Horton et al. 1990). Briefly, PCR products were made from the rKv2.1-pcDNA3 and pMT3 vector as a template, using appropriate primers and Pfu polymerase (25 cycles, 30 s at 95 °C, 30 s at 55 °C, and 1 min/kb at 72 °C, plus one cycle, 10 min at 72 °C). Second-round PCR was carried out using these fragments with the same PCR protocol and appropriate primers. The PCR products were digested with EcoRI and NotI and ligated into a similarly digested vector (pMT3).

ΔC-Kv2.1pMT3 was constructed by deleting residues 413 to 853 of rat Kv2.1 using the standard PCR overlap extension method as outlined previously. The PCR product was digested with ApaI and NotI and ligated into a similarly digested vector (rKv2.1-pMT3).

ΔCTA-Kv2.1pMT3 was constructed by deleting residues 741 to 853 of rat Kv2.1 using the standard PCR overlap extension method as outlined previously. The PCR product was digested with ApaI and NotI and ligated into a similarly digested vector (rKv2.1-pMT3). All constructs were confirmed by automated dideoxy sequencing.

Thereby, two mutants of the Kv2.1 channel were generated: Kv2.1ΔCTA lacks the CTA domain while Kv2.1ΔC lacks the entire C-terminus that comprises CTA and Kv2 domains. Each construct contains a point mutation to generate a 2,000-fold toxin binding enhancement (Goldstein and Miller 1992). A 1D4 immunoaffinity tag was added to the C-terminus to enable efficient immune-affinity purification (Sokolova et al. 2001).

Expression of Channel Protein We expressed the two mutants of the Kv2.1 channel in eukaryotic Vero cells. The cells were grown either on round cover glasses in a 6-well tissue culture plate (30•10³ cells per well) for 22–24 h in 2 ml of fresh complete medium (DMEM/High glucose, HyClone (USA)) or directly in 100 mm dishes (200•10³ cells per dish) in 8 ml of fresh complete medium (DMEM/High glucose, HyClone (USA)). The cells were transiently transfected with plasmid

pMT3, containing recombinant Kv2.1 channels, using the Metafecten™ PRO kit, according to the manufacturer's protocol. The transfection mixture was removed and replaced with fresh medium after 24 h and transfected cells were used for protein purification within 42–46 h after transfection. The transfection efficiencies were typically 50–60 %.

Purification of Channel Protein Truncated Kv2.1 channels were purified using the protocol established previously for the *Shaker* Kv channel (Sokolova et al. 2001). Briefly, the transfected Vero cells were solubilized for 1 h at 4 °C, using 2.5 % CHAPS in wash buffer (wash buffer contained 40 mM EDTA, 50 mM KCl, with 1 tablet of Pierce protease inhibitor cocktail per 10 ml of buffer). Insoluble cellular debris was pelleted using centrifugation for 10 min at 4,000×g at 4 °C. Then, 5 % glycerol and 50 mM NaCl were added to the supernatant. The extract was loaded onto a 1D4 immunoaffinity column (Oprian et al. 1987), incubated for 1 h, nonspecific binding was removed with excess wash buffer, and purified protein was eluted using the 1D4 peptide. To quantify the fraction of correctly folded channels, a modified protocol using radioactive labeled AgTx2 (Sokolova et al. 2001, 2003) was utilized. Briefly, [¹²⁵I]NEM-labeled AgTx2 was added to the elution fractions to a final concentration of 12.5 nM and, after 30-min of incubation on ice, the unbound toxin was separated from the protein–toxin complex on a Microcon filtering device (pore size 100 μm, Millipore).

Electron Microscopy and 3D Image Processing Freshly eluted protein (3 μl) was applied to carbon coated copper grids, subjected to negative glow-discharging at –20 mA for 45 s in an air atmosphere. Excess protein was then blotted off with filter paper, and grids were washed one time with wash buffer for 30 s. Negative image contrast was enhanced using 1 % uranyl acetate. Prepared grids were examined on the Philips Technai G12 (FEI) electron microscope at 120 kV and a 1.5–1.8 μm underfocus under the low-dose condition. Images were captured with an Eagle 4Kx4K digital camera (FEI) at 52,000x magnification. Obtained micrographs had a pixel size of 2.22 Å. Groups of 2×2 pixels were then averaged to give 4.44 Å per pixel on the micrograph. We picked 5417 single particle images of Kv2.1ΔCTA and 4979 single particle image of Kv2.1ΔC manually, using Signature software (Chen and Grigorieff 2007). To process the images, we used classification procedures implemented in IMAGIC (van Heel et al. 1996). We followed the standard protocol as described previously (Sokolova et al. 2001, 2003). Using the angular reconstitution method (Van Heel 1987), the relative orientations of the characteristic views were determined. Multivariate statistical analysis (MSA) on aligned particles produced eigen images (Supplemental

Fig. S1 c, g), that suggest that some particles have a 4-fold symmetry. This is clearly visible in eigen images #1 and #3 for Kv2.1ΔC and eigen image #4 for Kv2.1ΔCTA. The 2-fold symmetry, visible in eigen image #2 for Kv2.1ΔC, #2 and #3 for Kv2.1ΔCTA is probably caused by particles that correspond to the side views of the channels. The 3D reconstructions were calculated using the exact filter back projection algorithm (Harauz and van Heel 1986). Reprojections of the first 3D reconstructions were then used in a new round of multi-reference analysis (MRA) followed by MSA (van Heel and Stoffer-Meilicke 1985). These procedures (classification and reconstruction) were iterated five times for the Kv2.1ΔC channel and three times for the Kv2.1ΔCTA channel to refine class-images and corresponding Euler angles.

The micrographs were corrected for the CTF of the electron microscope, and 3D structures were further refined, using the FREALIGN (Grigorieff 2007). The resolution of the 3D reconstructions was estimated by dividing each data set into two subsets and calculating independent 3D maps, which were then compared by FSC with the resolution limit taken at the point where the FSC fell below 0.5 (Böttcher et al. 1997). The measured resolution coincides with the approximate positions of the first CTF zero. The docking of the crystal structures into obtained electron densities was realized using the UCSF Chimera (Pettersen et al. 2004). The difference maps between two truncated channel structures were calculated using Situs command *voldiff* (Wriggers 2010). The refining of the preliminary docking generated in UCSF Chimera, to the nearest maximum of the cross-correlation and determining the corresponding cross-correlation coefficients was performed using Situs command *collage*.

Homology Modeling and Fitting to the Electron Density The transmembrane part of the Kv2.1 channel model in open conformation was obtained using homology modeling based on the Kv1.2 crystal structure (PDB 2A79), while the model of the Kv2.1 channel in closed conformation was constructed based on the Kv1.2 closed structure obtained by Delemotte et al. (2011) using molecular dynamics simulations. Alignments of the templates and the target sequences were done with T-COFFEE (Notredame et al. 2000); structures of the Kv2.1 in open and closed states were built with MODELLER (Eswar et al. 2006), quaternary structures were visualized using UCSF Chimera (Pettersen et al. 2004).

Molecular Dynamics Both open and closed state models of the Kv2.1 channel were embedded into a solvated POPC lipid bilayer (as a model of a eukaryotic membrane), all ionizable residues were set to their ionization states expected at pH 7, potassium and chloride ions were added

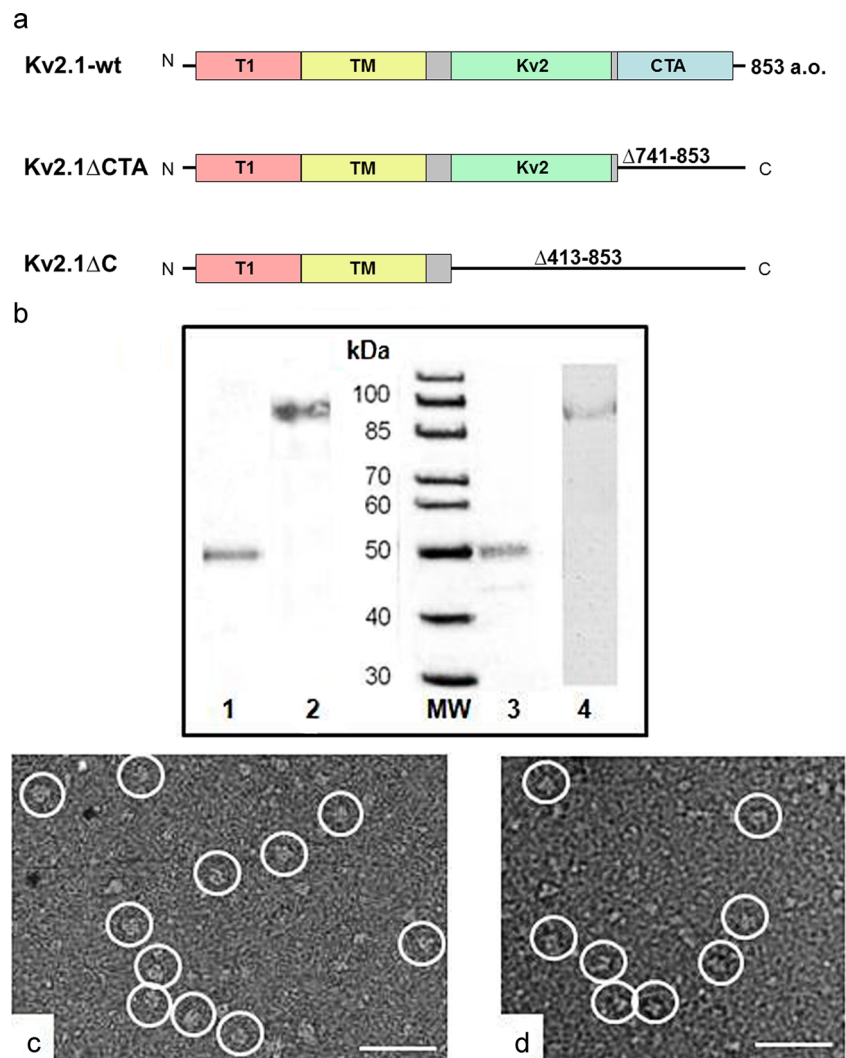
to the system up to concentrations of 150 mM. Next, a molecular mechanics model based on the CHARMM32 force field was constructed. The relaxation and simulations of the system with molecular dynamics were accomplished using the following protocol: at first protein and potassium ions inside the pore were fixed by Hooke's potential, with a force constant of $10 \text{ kkal/mol/\AA}^2$ to allow the relaxation of lipids and waters for 8 ns, after that the protein and ions were released and the simulations were run for 40 ns or more. VMD (Humphrey et al. 1996) and NAMD (Phillips et al. 2005) programs were used for system construction, simulation and analysis. The size of the simulation cell was $150 \times 150 \times 100 \text{ \AA}^3$. The following parameters were employed for the simulations: periodic boundary conditions, pressure coupling at 1 bar using Berendsen barostat in the direction normal to membrane, a temperature at 300 K was maintained via Langevin dynamics, the electrostatic interactions were computed with the Particle mesh Ewald method (Darden et al.

1993), 8 Å cutoff for the van-der-Waals interactions was used.

Results

Expression and Purification of Proteins We expressed two C-terminal mutants of the Kv2.1 channel (Kv2.1ΔCTA and Kv2.1ΔC) in Vero cells and purified the detergent-solubilized proteins on an immunoaffinity column using the 1D4 epitope-tag as described elsewhere (Sokolova et al. 2001). The Kv2.1ΔCTA mutant lacks 112 residues from the C-terminal end (Fig. 1a). The Kv2.1ΔC mutant lacks the entire C-terminus: 440 residues that include the C-terminal Kv2 and CTA domains and a S6-Kv2 linker (~50 aa) (Ju et al. 2003) (Fig. 1a). SDS-PAGE analysis and immunoblotting show single bands, corresponding to about 90 kDa for Kv2.1ΔCTA, and about 50 kDa for Kv2.1ΔC (Fig. 1b). The molecular

Fig. 1 The generation of Kv2.1 mutants and protein purification. **a** Schematic representation of the domain organization of Kv2.1 channel. FL – full-length, T1 – N-terminal tetramerization domain, Kv2 and CTA – C-terminal domains. **b** SDS-PAGE and Western blot analyses of purified Kv2.1 proteins. Lane 1 – western blot of the elution from the 1D4 column of Kv2.1ΔC. Lane 2 – western blot of the elution from the 1D4 column of Kv2.1ΔCTA. The monoclonal antibodies directed against the 1D4 tag were used as primary antibodies, and the polyclonal rabbit anti-mouse antibodies, labeled with alkaline phosphatase, as secondary antibodies. Lane 3 – Silver nitrate stained gel of the elution from the 1D4 column of Kv2.1ΔC. Lane 4 – Silver nitrate stained gel of the elution from the 1D4 column of Kv2.1ΔCTA. MW – molecular weights lane. **c** Image of negatively stained Kv2.1ΔCTA; **d** Image of negatively stained Kv2.1ΔC. White circles mark particles, used for further analysis (Bar 100 nm)



masses of Kv2.1 Δ CTA and Kv2.1 Δ C monomers have been predicted, according to the primary structure of the monomer to be ~83 kDa and ~52 kDa, correspondingly. The molecular mass observed in our experiments was slightly higher, ~90 kDa for Kv2.1 Δ CTA, and nearly equal to that predicted for Kv2.1 Δ C (Fig. 1b). In the case of the Kv2.1 Δ CTA, the difference may occur because of phosphorylation of the remaining part of the Kv2.1 C-terminus (Murakoshi et al. 1997) that can cause a large shift in molecular mass.

Toxin Assay Levels of expression and proper folding of the mutant and wild type Kv2.1 channels were examined using labeled AgTx2 (Goldstein and Miller 1992). The ability to bind radioactive labeled agitoxin proves the maintenance of the channel's tetrameric structure during isolation and purification. We have performed the toxin assays on the same elution fractions that were later used for EM analysis.

Briefly, the [125 I]NEM- AgTx2 solution was added to the elution fractions ($N=10$) or to the cell suspension ($N=25$) to a final concentration of 12.5 nM. Binding was performed at 4 °C for 30 min, after which the unbound toxin was separated from the protein–toxin complex using gel filtration on the C-25 SP-Sephadex resin (Sigma). Radioactivity was measured in a liquid scintillation counter. The [125 I]NEM- AgTx2 binding (Table 1) demonstrated that after the affinity purification about 30 % of active Kv2.1 channels remained in the solution, consistent with the previous result for the *Shaker* channel (Sokolova et al. 2001, 2003).

Electron Microscopy and Image Processing Both purified channel proteins exist as tetramers in solution. This was demonstrated by labeled toxin assays (Table 1), since the AgTx2 can reversibly bind only to correctly folded, tetrameric Kv channels (Gross and MacKinnon 1996; Goldstein and Miller 1992). The homogeneity of the purified proteins has been demonstrated by EM visualization of the single channel particles (Fig 1c, d). Statistical analysis revealed that single particles possess different orientations (Supplemental Fig. S1b, f). Some of the Kv2.1 Δ C particles (Supplemental Fig. S1b) have a preferential orientation with their channel axis perpendicular to the carbon film of the EM grid, in contrast with the full-length Kv2.1 particles, which were mainly oriented with their long axis parallel to the carbon film (Adair et al. 2008).

Single particle EM and IMAGIC were used for 3D image processing (Van Heel et al. 1996). Single images of mutant channels (Supplemental Fig. S1a, e) were band-pass filtered, aligned, first against the rotational average, then against a total sum of all previously aligned images. Stable classes were obtained after four iterations of alignment and reconstruction for Kv2.1 Δ CTA and six iterations for Kv2.1 Δ C. Some of the characteristic class-sum views for Kv2.1 Δ C and Kv2.1 Δ CTA are shown on Fig. 2a. The strongest classes were used for the calculation of preliminary 3D reconstructions using angular reconstitution (Van Heel 1987), without imposing a four-fold symmetry (Supplemental Fig. S1c, d). The obtained structures were further refined and corrected for CTF using FREALIGN (Grigorieff 2007). The C4 symmetry has been imposed on the final structures (Fig. 2b, c). The resulting structures of mutant channels have been determined at 2.0 nm resolution for Kv2.1 Δ C and 2.4 nm resolution for Kv2.1 Δ CTA (Supplemental Fig. S2). The chosen contour level based on an average protein density of 810 Da/nm³ (Matthews 1968) and volume corresponded to ~260 kDa for Kv2.1 Δ C and ~420 kDa for Kv2.1 Δ CTA. These volumes include the phosphorylation and about 15 kDa per subunit of bound detergent as estimated previously (Sokolova et al. 2001).

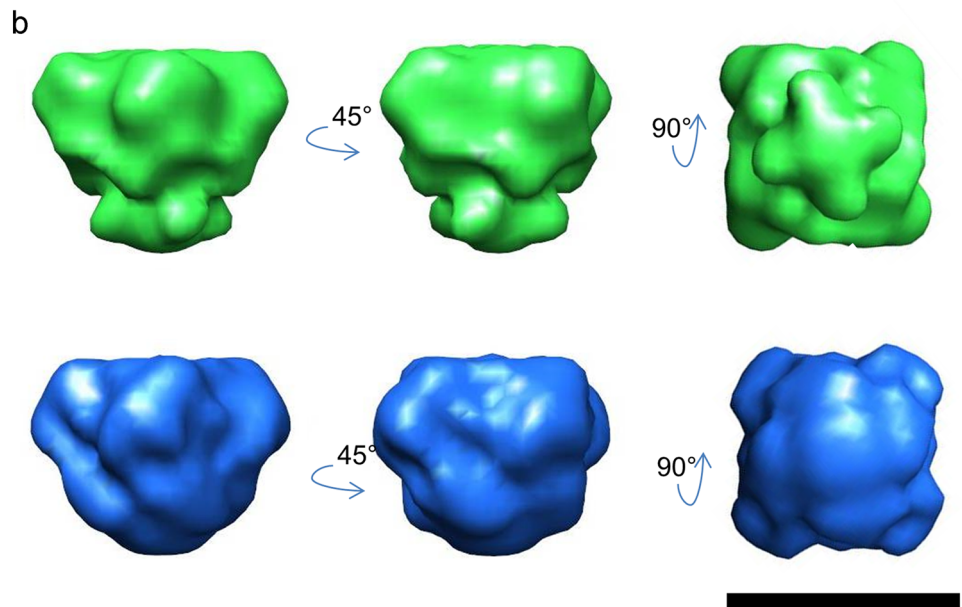
Overall 3D Structures of Truncated Kv2.1 Channels The overall structure of Kv2.1 Δ C possesses the pronounced ‘mushroom’ shape (Fig. 2b), similar to that of the Kv1.1 channel (Sokolova et al. 2001, 2003; Orlova et al. 2003). The 3D structure is ~80 Å in height and is clearly divided into two structural parts: the larger upper domain (diameter ~80 Å, thickness ~50 Å) and the smaller bottom domain (diameter ~35 Å, thickness about 30 Å) separated with a sharp contraction in the middle (diameter ~40 Å). The top surface of the upper part is flat, unlike the prominent top surface of the Kv1.1 channel (Sokolova et al. 2001). The 3D structure of the full length Kv2.1 also has a flat upper surface (Adair et al. 2008) in agreement with our data. It is known that the Kv2.1 channel lacks the N- glycosylation (Shi and Trimmer 1999). Taking into account the fact that the reconstruction of an experimentally decylosylated Kv1.1 channel also possesses a flat top surface (O.Sokolova, unpublished data), we concluded that the upper domain of the presented 3D structure is the membrane-embedded domain.

Table 1 Labeled AgToxin2 binding to the functional Kv2.1 channels expressed in Vero cells, and to the purified channel protein

Sample	AgTx2-[125 I] bound to whole cell surface, Pmol/plate ($N=25$)	AgTx2-[125 I] bound to purified protein, Pmol/plate ($N=10$)
Kv2.1, full length	1.05±0.12	0.34±0.03
Kv2.1 Δ CTA	0.79±0.1	0.18±0.03
Kv2.1 Δ C	0.66±0.008	0.24±0.015

Fig. 2 Single particle image analysis and reconstruction of the 3D structure of truncated Kv2.1 channels. **(a)** Image processing of (left column) Kv2.1 Δ C and (right column) Kv2.1 Δ CTA: (top line) typical class-averages, used for reconstruction, (middle line) reprojections of 3D structures, (bottom line) 3D structures, processed in IMAGIC. Final 3D reconstructions processed in FREALIGN of **(b)** Kv2.1 Δ C, and **(c)** Kv2.1 Δ CTA. For each reconstruction two side views (differ by 45° from each other) and a bottom view are shown. The bar size is 10 nm

a	Kv2.1 Δ C	Kv2.1 Δ CTA
classes		
reprojections		
3D volumes		



Thus, the bottom part of the reconstruction is the cytoplasmic domain. It has four ‘protuberances’, which are rotated by $\sim 60^\circ$ relative to the upper part. The Kv2.1 Δ C completely lacks its C-terminus, therefore the cytoplasmic part represents only the N-terminal T1 domain. Unlike the low resolution reconstructions of other Kv channels (Sokolova et al. 2001, 2003, 2012; Orlova et al. 2003; Kim et al. 2004) the 3D reconstruction of the Kv2.1 Δ C lacks the distinct ‘windows’ between the membrane-embedded and the T1 domains, which was thought to be the characteristic feature of all Kv channels. It should be noted that the published 3D reconstruction of the full-length Kv2.1 channel at 2.5 nm resolution (Adair et al. 2008) also lacks the ‘windows’, in agreement with our present structure.

The overall 3D structure of the Kv2.1 Δ CTA (Fig. 2c) possesses a roughly pyramidal shape with rounded corners and a height of ~ 80 Å, a diameter of the top part of ~ 80 Å, and a diameter of the bottom part of ~ 50 Å. The top

surface of the structure is flat, similar to that of the Kv2.1 Δ C (Fig. 2b). The bottom part of Kv2.1 Δ CTA is much larger, with massive protrusions, likely representing the remaining Kv2 domains. The top part of this mutant is rotated by 60° relative to the bottom part, similar to the Kv2.1 Δ C structure. No pronounced ‘windows’ between the membrane-embedded and the cytoplasmic parts of the reconstruction were detected.

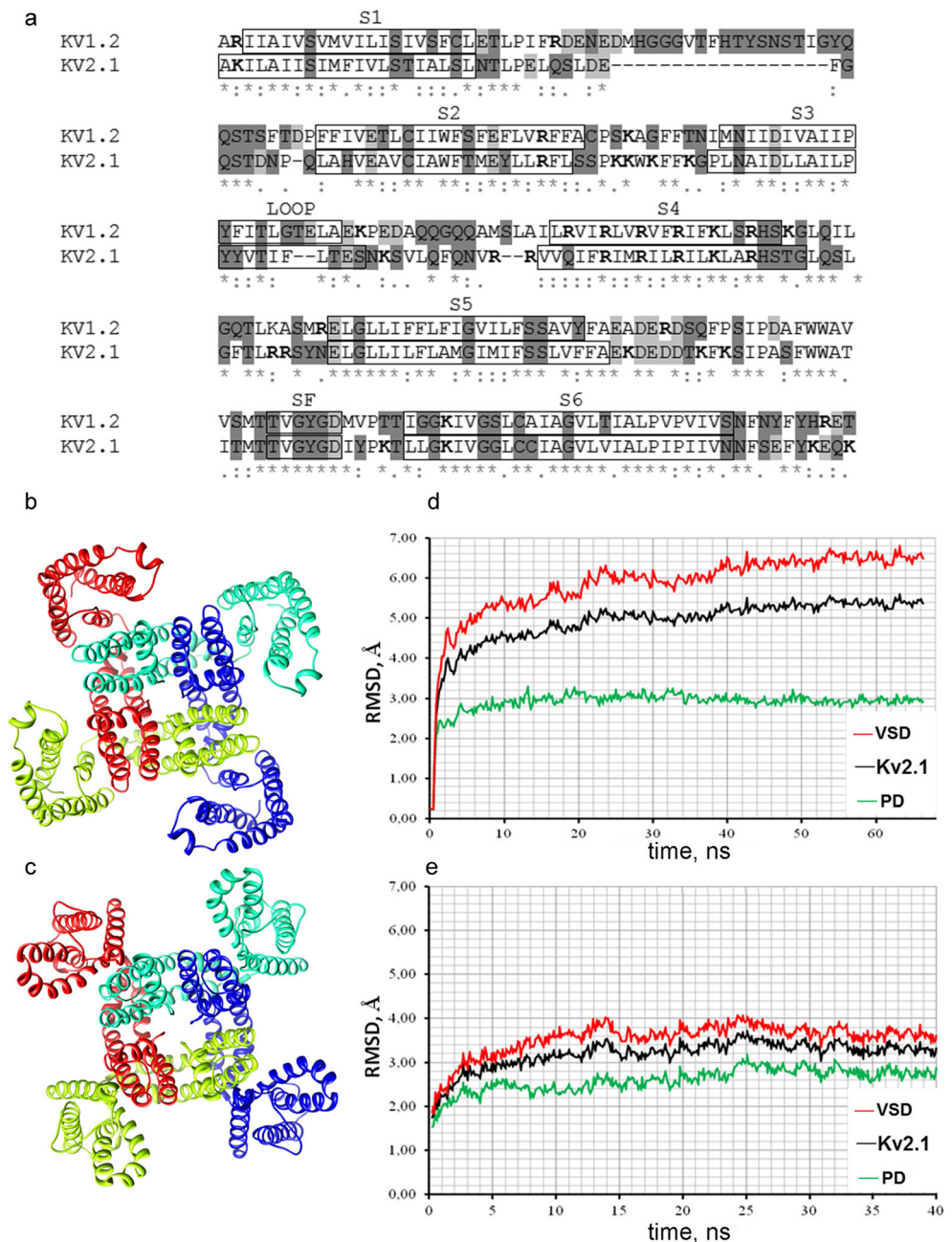
Homology Modeling of the Kv2.1 Voltage-Gated Potassium Channel in Open and Closed States Kv2.1 shares a high percentage of identity with Kv1.2 (~ 55 % overall and ~ 60 – 70 % in helices) (Fig. 3a). Therefore the available crystal structure of Kv1.2 (PDB code 2A79, transmembrane chain, residues 161–421) and the model of Kv1.2 in closed state, generously provided by Dr. M.Tarek (Delemotte et al. 2011) were used as templates for homology modeling. Using homology modeling two structural models of Kv2.1 in its closed (Fig. 3b) and open (Fig. 3c) states were built.

Molecular Dynamics Simulations of the Kv2.1 Voltage-Gated Potassium Channel in Open and Closed States Molecular models of Kv2.1 channels in open and closed states, obtained by homology modeling, were embedded into a hydrated POPC lipid bilayer. The trajectories of molecular dynamics (MD) simulations allow comparing the structure and conformational dynamics between open and closed states at atomic levels of detail. The structural changes of Kv2.1 in closed and open states were monitored through the evolution of root mean square deviation (RMSD) of C α atom positions and are shown in Fig. 3d and e, respectively. RMSDs were calculated for the whole membrane-embedded domain, the pore

region (377–382 aa) and the voltage-sensor domain (VSD). Helices S1 to S4 (187–316 aa) were calculated separately to elucidate the flexibility of the regions upon the opening of the channel.

In the course of the simulations, the RMSD of the whole protein increases during the first nanoseconds of the simulations and then fluctuates within the range of 0.37–0.55 nm for the closed state conformation (Fig. 3d), and 0.27–0.37 nm for the open state conformation (Fig. 3e). This initial jump in RMSD is presumed to reflect the relaxation of the protein upon transfer to a bilayer environment. The RMSDs have a non-diverging

Fig. 3 Molecular homology modeling and MD simulations of the Kv2.1 channel in open and closed states. **(a)** Alignment of the Kv2.1 channel (residues 188–424) with the Kv1.2 crystal structure (PDB 2A79) (residues 161–421). The framed regions: S1, S2, S3, Loop, S4, S5, the selectivity filter, S6 (positive charged - bold, negative charged - on a light gray background, hydrophilic - on dark gray background, hydrophobic - black). Models of the quaternary structure of the Kv2.1 channel in closed **(b)** and open **(c)** conformations (Top view). Blue, cyan, yellow, red are for subunits A, B, C, and D respectively. RMSD of C α of the whole channel (black curve), pore part (green curve) and voltage sensor part (red curve) of the channel Kv2.1 in closed **(d)** and open **(e)** conformations



trend at the end of the simulations, thus, confirming that the system has reached its equilibrium state.

Discussion

The Kv2.1 channel is a member of the *Shab* ion channels subfamily (reviewed in Pischalnikova and Sokolova 2009). These channels are characterized by their large cytoplasmic C-termini (440 aa) that carry out many important functions: voltage-dependent gating (Ju et al. 2003), the channel's polarized expression determination, clustering (Lim et al. 2000), and the regulating of activation of the channel's properties by C-terminal phosphorylation (Park et al. 2005). According to the previous mutagenic and MD simulation experiments, the C-termini of Kv2.1 are divided into two large domains: Kv2 and CTA (Ju et al. 2003). The CTA domain was predicted to be the 741–853 residues of the channel's C-terminus, while the Kv2 domain occupies the residues from 461 to 711 (Supplemental Fig. S3) (Ju et al. 2003). The low resolution 3D structure of the full-length human recombinant Kv2.1 channel, purified from CHO cells was previously published (Adair et al. 2008). Authors docked the available crystal structure of Kv1.2 (Long et al. 2005) into the obtained electron density. Noticeably, it leaves a large unoccupied space on the sides and below the T1 domain. It has been proposed that C-terminal domains can account for these extra-densities (Adair et al. 2008; Wray 2009).

To check this hypothesis we have constructed two C-terminal deletion mutants of Kv2.1: Kv2.1 Δ CTA, lacking the residues from 741 to 853 and Kv2.1 Δ C, lacking the residues from 413 to 853 (Fig. 1a). We have purified both C-terminal deletion mutants using affinity chromatography (Fig. 1b). Toxin binding (Table 1) proved that truncation of the Kv2.1 channel yields correctly folded proteins, since the AgTx2 reversibly binds only to tetrameric Kv channels (Gross and MacKinnon 1966; Goldstein and Miller 1992).

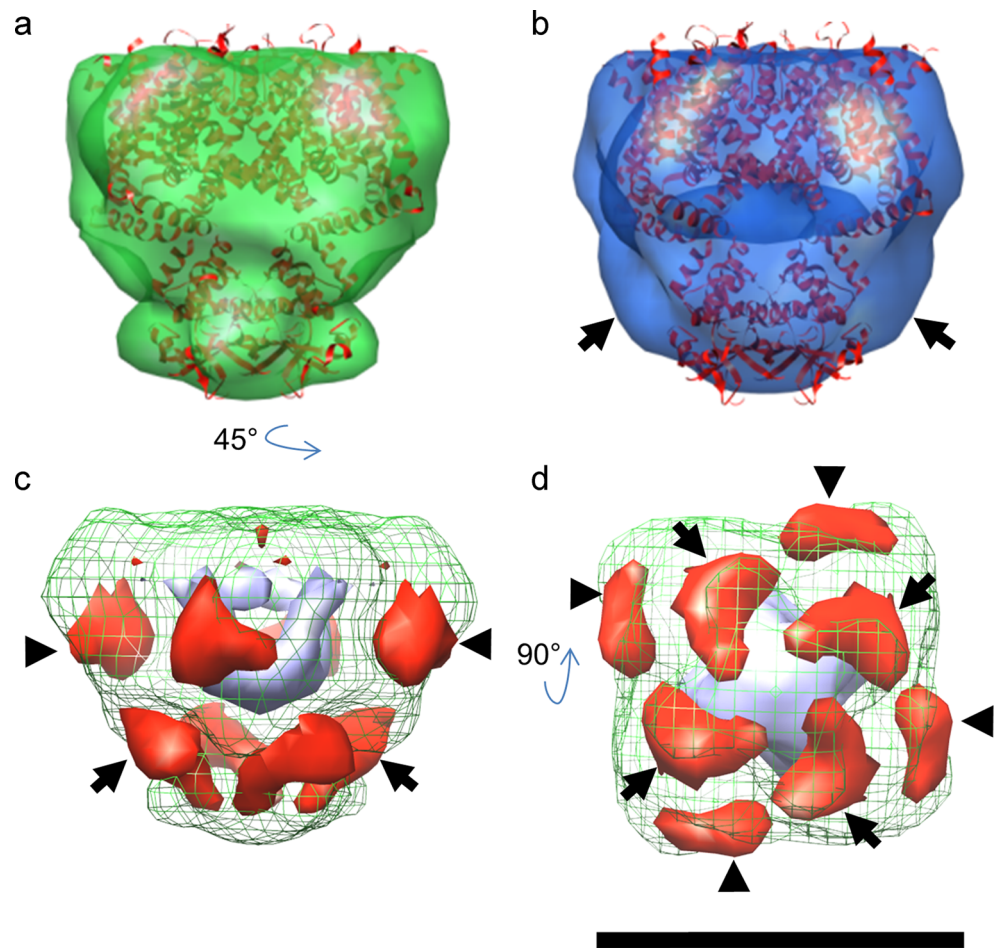
Overall Structure of Mutant Channels We used 3D EM and single particle analysis to calculate 3D maps of truncated Kv2.1 Δ C (Fig. 2b) and Kv2.1 Δ CTA channels (Fig. 2c) at the resolution of 2.0 and 2.4 nm, respectively (Supplemental Fig. S2). Removing the large C-termini revealed the typical 'mushroom' shape of the channel with one larger and one smaller domain (Fig. 2b). Docking the available full-length Kv1.2 crystal structure with the β -subunit detached (Long et al. 2005) clearly demonstrated that the larger domain in both reconstructions is membrane-embedded, while the smaller is the cytoplasmic domain (Fig. 4a, b). The smaller domain of Kv2.1 Δ CTA possesses a more square shape, compared to that of Kv2.1 Δ C and has four large extra-densities on all sides of the T1 domain (Fig. 4b, black arrows). The characteristic

two-layer architecture is common in a large number of tetrameric ion channels, not only of eukaryotic (Kim et al. 2004; Sokolova et al. 2001, 2012; Orlova et al. 2003; Ludtke et al. 2011), but also prokaryotic (Uysal et al. 2009) origin. It is called a 'hanging gondola' and allows the large N-terminal inactivation peptide to reach the inner pore of the channel for inactivation (Kobertz et al. 2000). The classical 'hanging gondola' structure consists of two domains, separated by thin linkers that border the 'windows' between them. In the published 3D structure of the full-length Kv2.1 channel (Adair et al. 2008) no 'windows' between the membrane-embedded and the cytoplasmic domains were detected. It has been suggested that in the full-length Kv2.1 channel, they may be concealed by large C-terminal domains. Unexpectedly, removing the entire C-terminus did not help us visualize the prominent 'windows'. Since the Kv2.1 channel does not have an inactivation peptide (Adair et al. 2008), these 'windows' do not need to serve as controlling filters for the inactivation peptide to access the pore (Gulbis et al. 2000). Therefore the size of the 'windows' is not substantial, comparing to other Kv channels (Kim et al. 2004; Sokolova et al. 2012).

Structure of the Membrane-Embedded Domain Thus we revealed that the larger domain within our reconstructions is the membrane-embedded domain (Fig. 4a, b). In both 3D reconstructions of truncated channels (Fig. 5b, c), it possesses all the characteristic structural features of a wild type Kv2.1 membrane domain (Fig. 5a): namely, the overall dimensions, the flat top surface and the presence of the smaller subdomains: M1 to M3. The presence of smaller subdomains within the membrane-embedded domain is another characteristic feature of Kv channels (Sokolova et al. 2003).

Despite the great similarity in the membrane parts of these mutant channels, they differ slightly from each other. When looking from the extracellular side, the membrane part of the Kv2.1 Δ CTA structure has an almost square configuration (top view of the channel at Fig. 6c, second from the left at the bottom). The Kv2.1 Δ C structure, from the same point of view, possesses four pronounced left-twisted blades (Fig. 6c, bottom right). This observation provides reasons to assume that the removal of the C-terminal domain of the Kv2.1 channel may alter the conformation of the membrane domain. Although the obtained resolution does not allow us to make a detailed characterization of conformational differences in membrane domains of mutant channels, previous experimental data demonstrates that channel opening lead to conformational rearrangements in the membrane domain. Particularly, the MD simulations of the Kv1.2 open and closed states (Han and Zhang 2008; Delemotte et al. 2011; Jensen et al. 2012) revealed a translation of the S3 and especially S4 helices during the opening of the channel. As a result, the overall shape of the whole transmembrane domain might change dramatically. It is well accepted that there are at least two

Fig. 4 An interpretation of 3D EM densities of truncated Kv2.1 channels. Docking the crystal structure of the Kv1.2 channel (red) (Long et al. 2005) into the EM densities of (a) Kv2.1ΔC (side view), (b) Kv2.1ΔCTA (side view). Black arrows are pointing to the extra densities on the sides of a T1 domain in a Kv2.1ΔCTA reconstruction. (c) Difference map between Kv2.1ΔCTA and Kv2.1ΔC (positive densities – red, negative densities – blue), superimposed onto a 3D structure of a Kv2.1ΔC (green), side view. (d) The same map as in (c), bottom view. Black arrows are pointing to the extra densities on the sides of T1 domains, black arrowheads are pointing to the extra-densities close to the M2 subdomain. The bar size is 10 nm



stable states of the transmembrane domain: open and closed (Pathak et al. 2007; Vargas et al. 2011). Therefore, the difference between the mutants' transmembrane parts might stem from the fact that one of them is open, and other is closed. This hypothesis, however, must be verified by other methods.

MD Simulations of the Kv2.1 Open and Closed States In order to investigate possible conformational changes in the membrane-embedded domain upon the Kv2.1's activation we performed MD simulations of the Kv2.1 open and closed states, embedded in the lipid bilayer (Fig. 3d, e).

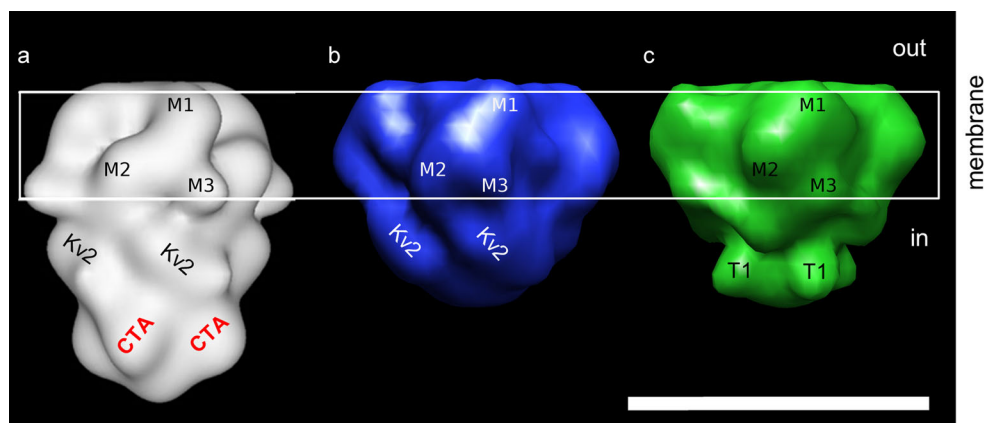


Fig. 5 Localization of cytoplasmic C-terminal domains within mutant Kv2.1 channels. a The 3D structure of the Kv2.1 full length channel (generously provided by Dr. B.Adair); b The 3D structure of the Kv2.1ΔCTA channel; c The 3D structure of the Kv2.1ΔC channel. All

channels are depicted in the same orientation (side view). The locations of the C-terminal Kv2 and CTA and N-terminal T1 domains are marked. The lipid membrane is shown as a white rectangle. Bar size is 10 nm

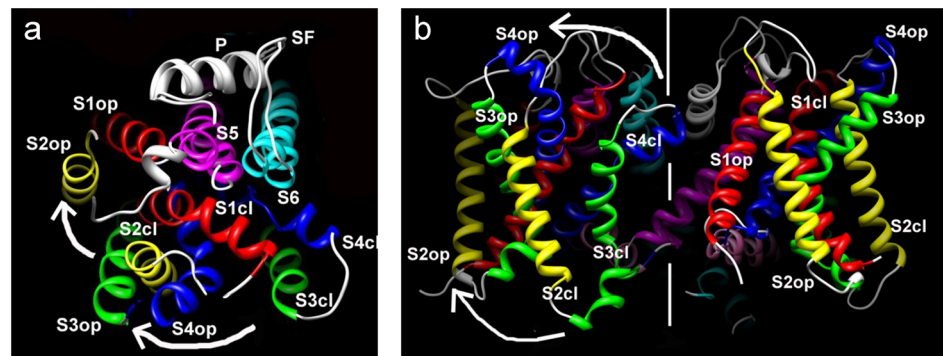
The crystal structure of the Kv1.2 revealed the atomistic architecture of the VSD in an open state of the channel (Long et al. 2005). This structure was used to prepare a model of the Kv2.1 channel by homology modeling. The sequence alignment between Kv2.1 (residues 188–424) and Kv1.2 (shown in Fig. 3a) indicates a high level of homology between structurally important regions (including charged residues), thus the performed alignment is unambiguous.

We employed MD simulations in atomic detail to investigate the movements of the helices within the transmembrane part of the Kv2.1 channel while transferring from closed to open state. The S4 helix in each VSD contains five conserved positively charged residues, located at every third position. The S4 charges are responsible for most of the gating charge movement during activation (Tombola et al. 2006). The conserved Gly in the loop between S4, S5 and S6 can produce swivel motions and make these regions more flexible (Labro et al. 2008). Because of a lack of a side chain, glycine has a large degree of freedom of rotation about the phi psi dihedral angles and can introduce conformational flexibility in the S4 helix.

The obtained molecular models of Kv2.1 in closed and open states (Fig. 3b, c) were superimposed, and aligned using

the selective filter position as an anchor point (Fig. 6a, b). It has been shown in MD studies with potassium channels in closed and open conformations that the position of the selective filter does not change dramatically upon opening of the channel (Haliloglu and Ben-Tal 2008). The comparison of the two models revealed a swivel movement of the entire S1–S4 helix bundle upon the opening of the channel (white arrows on Fig. 6a). As expected, the largest movement occurs in the S4 helix, which moves outward to the tilted position, similar to that shown in the crystal structure of the open Kv1.2/2.1 channel chimera (Long et al. 2007). The movement of the S4 helix subsequently pulls up the S3–S4 linker, causing it to tilt towards the extracellular part of the membrane (Fig. 6b). All these rearrangements result in changing the overall shape of the open channel, compared to the closed one. In order to check these possible changes between the Kv2.1 conformations we produced low-resolution maps (2.0 nm) of both models using UCSF Chimera (Pettersen et al. 2004) (Fig. 6c, upper panel). This analysis has revealed that even at a 2.0 nm resolution the overall changes in the membrane-embedded domain upon channel activation might be detected. Moreover, comparing these models with the mutants' 3D structures indicated some similarity in the membrane-

Fig. 6 Modeling of conformational changes in the membrane-embedded domain upon removing the C-terminus of the Kv2.1 channel. The superimposed structural models of open and closed Kv1.2 channels, obtained after homology modeling and MD simulations in the lipid bilayer: **a** one quarter of the tetramer, top view; **b** an entire membrane-embedded part, side view. The positions of transmembrane helices in the open model are marked: S1op, S2op, etc.; the positions of helices in the closed model are marked: S1cl, S2cl, etc. The white arrows mark the directions of the swivel motion upon the opening. P – pore domain, SF – selectivity filter. **c** Comparison of the low-resolution structural models in closed (*left*) and open (*right*) states (*top panel*) with the 3D reconstructions of Kv2.1 Δ CTA (*left*) and Kv2.1 Δ C (*right*) channels (*bottom panel*)



C	closed		open	
	side view	top view	side view	top view
MD Model				
EM map				
	Kv2.1 Δ CTA		Kv2.1 Δ C	

Table 2 The results of docking the atomic models of Kv1.2 and Kv2.1 in open and closed states into the 3D electronic densities of truncated Kv2.1 channel (Correlation coefficients of the best match)

3D structure	Kv1.2 (Long et al. 2005)	Model Kv2.1 open	Model Kv2.1 close
Kv2.1 Δ CTA	0.60	0.64	0.67
Kv2.1 Δ C	0.58	0.65	0.64

embedded part of the latter. (Fig. 6c). Thus, the comparison of the closed model to the 3D structure of Kv2.1 Δ CTA and the open model to the 3D structure of Kv2.1 Δ C (Fig. 6c) revealed better correlation, when compared to the docking results using the original Kv1.2 crystal structure (Long et al. 2005) (Table 2). While the transmembrane part of the Kv2.1 model in the closed state has a square shape, similar to Kv2.1 Δ CTA, the membrane part of the Kv2.1 model in the open state has characteristic paddles, similar to what might be seen in the Kv2.1 Δ C structure (Fig. 6c). Thus, we hypothesize that the obtained structures of Kv2.1 channel mutants may reflect different conformations of the channel; though obtaining the structures with the higher resolution is required for verification of this hypothesis.

Supporting our observations, several previous studies demonstrated that the deletion of the Kv2.1 C-terminus domain leads to a higher probability of the channel to adopt an open conformation. The truncation of the Kv2.1 channel at residue 535 exhibits a more hyperpolarized voltage-dependence of activation and an increased speed of activation compared to the full-length Kv2.1 (VanDongen et al. 1990; Murakoshi et al. 1997). The experimental dephosphorylation of the channel provides a similar effect (Murakoshi et al. 1997; Mohapatra and Trimmer 2006; Mohapatra et al. 2008). Removing the entire C-terminus of the Kv2.1 channel (Park et al. 2005) enables a more rapid activation of the channel.

Revealing the Cytoplasmic C-Terminal Subdomains in Kv2.1 Finally, we addressed the main question that remains unanswered in the previously published study of the full-length Kv2.1 structure (Adair et al. 2008) which is, how are the C-terminal Kv2 and CTA domains located with respect to one another and to the rest of the channel? To determine the spatial locations of the C-terminal domains we first compared the overall 3D reconstructions of the truncated channels to the available reconstruction of the full-length human Kv2.1 channel (Fig. 5). This comparison clearly demonstrated that a large bottom part is missing from both 3D structures of the truncated channels (Fig. 5b, c). Therefore we concluded that this is the tetramer of CTA domains (marked CTA on Fig. 5a). It was hypothesized previously (Ju et al. 2003), that CTA domains are located on the symmetry axis of the channel, in contact with other cytoplasmic domains, in agreement with our present data. The difference map between the 3D structures of Kv2.1 Δ CTA and Kv2.1 Δ C has been calculated using Situs (Wriggers 2010) and revealed that the Kv2.1 Δ C structure

additionally lacks four separated densities from its cytoplasmic part, just outside the tetramerization T1 domain (Fig. 4c, d, black arrows). Thus, these densities can be allocated to the Kv2 domains (marked Kv2 on the Fig. 5a, b). The earlier hypotheses suggesting that the cytoplasmic domains in the Kv2.1 not only surround the T1 domain (Adair et al. 2008), but also occupy the entire space below it (Ju et al. 2003) are in complete agreement with our findings.

Conclusions

A large number of protein structures have been solved in the past several decades by X-ray crystallography and NMR, providing detailed information for the understanding of protein folding, enzymatic catalysis, and intermolecular contacts. Yet, for the full-length eukaryotic ion channels, very few molecular structures have been solved (some examples are: Miyazawa et al. 2003; Long et al. 2005, 2007; Miller and Long 2012). Here we employed an integrative approach to obtain structural models of Kv ion channels using single particle EM and MD simulations and to reveal the possible conformational changes in the channel. Using this approach, we have, for the first time, obtained the 3D structures of truncated rat Kv2.1 channels. The obtained structures revealed the positions of large C-terminal domains: Kv2 and CTA. The Kv2 domains surround the N-terminal T1 domain, while the CTA domains occupy the entire space below it. These domains clearly interact with each other. MD simulation and homology modeling allowed us to compare the open and closed models of the Kv2.1 channel to our 3D reconstructions and to suggest different conformations for open and closed channels. The obtained results provided a new insight into inter-domain interactions in Kv2.1 channels and may serve as starting points for new MD and physiological experiments.

Acknowledgments Authors thank Prof. C. Miller for the generous gift of the AgTx2 expression construct, Prof. B. Adair for providing the 3D EM map of the full-length Kv2.1 and Prof. M. Tarek for the model of Kv1.2 in closed state. We also like to thank Dr. A. Shaytan for help with MD experiments, E. Trifonova, C. Williams and K. Piasta for proof-reading the manuscript. The EM studies were performed at the User Facilities Center “Structural Diagnostics of Materials” at the A.V. Shoubnikov Institute of Crystallography RAS in Moscow, Russia. This work was supported by the FP7 program EDICT - EUROPEAN DRUG INITIATIVE ON CHANNELS AND TRANSPORTERS (#201924), and Federal programs of Russian ministry of education and

science (#14.740.11.0255 and #14.740.11.0760). AG is supported by the Saint Petersburg State University project (#1.50.1038.2014). This article is dedicated to the memory of our good friend and colleague Dennis Wray.

Conflict of Interest The authors declare no conflict of interests.

References

- Adair B, Nunn R, Lewis S, Dukes I, Philipson L, Yeager M (2008) Single particle image reconstruction of the human, recombinant Kv2.1 channel. *Biophys J* 4:2106–2114
- Antonucci DE, Lim ST, Vassanelli S, Trimmer JS (2001) Dynamic localization and clustering of dendritic Kv2.1 voltage-dependent potassium channels in developing hippocampal neurons. *Neuroscience* 108:69–81
- Böttcher B, Kiselev NA, Stel'mashchuk VY, Perevozchikova NA, Borisov AV, Crowther RA (1997) Three-dimensional structure of infectious bursal disease virus determined by electron cryomicroscopy. *J Virol* 71:325–330
- Chen JZ, Grigorieff N (2007) SIGNATURE: a single-particle selection system for molecular electron microscopy. *J Struct Biol* 157:168–173
- Chung JJ, Li M (2005) Biochemical characterization of the native Kv2.1 potassium channel. *FEBS J* 272:3743–3755
- Darden T, York D, Pedersen L (1993) Particle mesh Ewald: an $N \cdot \log(N)$ method for Ewald sums in large systems. *J Chem Phys* 98:10089–10092
- Delemotte L, Tarek M, Klein ML, Amaral C, Treptow W (2011) Intermediate states of the Kv1.2 voltage sensor from atomistic molecular dynamics simulations. *Proc Natl Acad Sci U S A* 108(15):6109–6114
- Du J, Tao-Cheng JH, Zerfas P, McBain CJ (1998) The K⁺ channel, Kv2.1, is apposed to astrocytic processes and is associated with inhibitory postsynaptic membranes in hippocampal and cortical principal neurons and inhibitory interneurons. *Neuroscience* 84: 37–48
- Eswar N, Webb B, Marti-Renom MA, Madhusudhan MS, Eramian D, Shen MY, Pieper U, Sali A (2006) Comparative protein structure modeling using Modeller. *Curr Protoc Bioinformatics* Oct;Chapter 5:Unit 5.6. doi: 10.1002/0471250953.bi0506s15
- Goldstein SAN, Miller C (1992) A point mutation in a Shaker K1 channel changes its charybdotoxin binding site from low to high affinity. *Biophys J* 62:5–7
- Grigorieff N (2007) FREALIGN: high-resolution refinement of single particle structures. *J Struct Biol* 157:117–125
- Gross A, MacKinnon R (1966) Agitoxin footprinting the shaker potassium channel pore. *Neuron* 16(2):399–406
- Gross A, MacKinnon R (1996) Agitoxin footprinting the shaker potassium channel pore. *Neuron* 16:399–406
- Gulbis JM, Zhou M, Mann S, MacKinnon R (2000) Structure of the cytoplasmic beta subunit-T1 assembly of voltage-dependent K⁺ channels. *Science* 289:123–127
- Gutman GA, Chandy KG, Grissmer S, Lazdunski M, McKinnon D, Pardo LA, Robertson GA, Rudy B, Sanguinetti MC, Stühmer W, Wang X (2005) International union of pharmacology. LIII. Nomenclature and molecular relationships of voltage-gated potassium channels. *Pharmacol Rev* 57:473–508
- Haliloglu T, Ben-Tal N (2008) Cooperative transition between open and closed conformations in potassium channels. *PLoS Comput Biol* 4(8):e1000164
- Han M, Zhang JZ (2008) Molecular dynamic simulation of the Kv1.2 voltage-gated potassium channel in open and closed state conformations. *J Phys Chem B* 112:16966–16974
- Harauz G, van Heel M (1986) Exact filters for general geometry of three-dimensional reconstruction. *Optik* 73:146–156
- Horton RM, Cai ZL, Ho SN, Pease LR (1990) Gene splicing by overlap extension: tailor-made genes using the polymerase chain reaction. *Biotechniques* 8:528–535
- Humphrey W, Dalke A, Schulten K (1996) VMD - visual molecular dynamics. *J Mol Graph* 14:33–38
- Jensen MØ, Jogini V, Borhani DW, Leffler AE, Dror RO, Shaw DE (2012) Mechanism of voltage gating in potassium channels. *Science* 336(6078):229–233
- Ju M, Stevens L, Leadbitter E, Wray D (2003) The roles of N- and C-terminal determinants in the activation of the Kv2.1 potassium channel. *J Biol Chem* 278:12769–12778
- Kim LA, Furst J, Gutierrez D, Butler MH, Xu C, Goldstein SA, Grigorieff N (2004) Three-dimensional structure of Ito: Kv4.2-KChIP2 ion channels by electron microscopy at 21 Å resolution. *Neuron* 41: 13–19
- Kobertz WR, Williams C, Miller C (2000) Hanging gondola structure of the T1 domain in a voltage-gated K⁽⁺⁾ channel. *Biochemistry* 39: 10347–10352
- Kobrinsky E, Stevens L, Kazmi Y, Wray D, Soldatov NM (2006) Molecular rearrangements of the Kv2.1 potassium channel terminus associated with voltage gating. *J Biol Chem* 281:19233–19240
- Kreusch A, Pfaffinger PJ, Stevens CF, Choe S (1998) Crystal structure of the tetramerization domain of the Shaker potassium channel. *Nature* 392:945–948
- Labro AJ, Raes AL, Grottesi A, Van Hoorick D, Sansom MSP, Snyders DJ (2008) Channel gating requires a compatible S4-S5 linker and bottom PART of S6, constrained by non-interacting residues. *J Gen Physiol* 132(6):667–680
- Lim ST, Antonucci DE, Scannevin RH, Trimmer JS (2000) A novel targeting signal for proximal clustering of the Kv2.1 K⁺ channel in hippocampal neurons. *Neuron* 25:385–397
- Long SB, Campbell EB, Mackinnon R (2005) Crystal structure of a mammalian voltage-dependent Shaker family K⁺ channel. *Science* 309:897–903
- Long SB, Tao X, Campbell EB, MacKinnon R (2007) Atomic structure of a voltage-dependent K⁺ channel in a lipid membrane-like environment. *Nature* 450:376–382
- Ludtke SJ, Tran TP, Ngo QT, Moiseenkova-Bell VY, Chiu W, Serysheva II (2011) Flexible architecture of IP3R1 by Cryo-EM. *Structure* 19(8):1192–1199
- MacDonald PE, Ha XF, Wang J, Smukler SR, Sun AM, Gaisano HY, Salapatek AM, Backx PH, Wheeler MB (2001) Members of the Kv1 and Kv2 voltage-dependent K⁽⁺⁾ channel families regulate insulin secretion. *Mol Endocrinol* 15:1423–1435
- Malin SA, Nerbonne JM (2002) Delayed rectifier K⁺ currents, IK, are encoded by Kv2 alpha-subunits and regulate tonic firing in mammalian sympathetic neurons. *J Neurosci* 22:10094–10105
- Matthews BW (1968) Solvent content of protein crystals. *Mol Biol* 33: 491–497
- Miller AN, Long SB (2012) Crystal structure of the human two-pore domain potassium channel K2P1. *Science* 335:432–436. doi: 10.1126/science.1213274
- Miyazawa A, Fujiyoshi Y, Unwin (2003) N Structure and gating mechanism of the acetylcholine receptor pore. *Nature* 423: 949–955
- Mohapatra DP, Trimmer JS (2006) The Kv2.1 C terminus can autonomously transfer Kv2.1-like phosphorylation-dependent localization, voltage-dependent gating, and muscarinic modulation to diverse Kv channels. *J Neurosci* 26:685–695

- Mohapatra DP, Siino DF, Trimmer JS (2008) Interdomain cytoplasmic interactions govern the intracellular trafficking, gating, and modulation of the Kv2.1 channel. *J Neurosci* 28:4982–4994
- Murakoshi H, Trimmer JS (1999) Identification of the Kv2.1 K⁺ channel as a major component of the delayed rectifier K⁺ current in rat hippocampal neurons. *J Neurosci* 19:1728–1735
- Murakoshi H, Shi G, Scannevin RH, Trimmer JS (1997) Phosphorylation of the Kv2.1 K⁺ channel alters voltage-dependent activation. *Mol Pharmacol* 52(5):821–828
- Notredame C, Higgins DG, Heringa J (2000) T-coffee: a novel method for fast and accurate multiple sequence alignment. *J Mol Biol* 302(1): 205–217
- Oprian DD, Molday RS, Kaufman RJ, Khorana HG (1987) Expression of a synthetic bovine rhodopsin gene in monkey kidney-cells. *Proc Natl Acad Sci U S A* 84:8874–8878
- Orlova EV, Papakosta M, Booy FP, van Heel M, Dolly JO (2003) Voltage-gated K⁺ channel from mammalian brain: 3D structure at 1.8 Å of the complete (α)₄(β)₄ complex. *J Mol Biol* 326: 1005–1012
- Papazian DM (1999) Potassium channels: some assembly required. *Neuron* 23:7–10
- Park KS, Mohapatra DP, Misonou H, Trimmer JS (2005) Graded regulation of the Kv2.1 potassium channel by variable phosphorylation. *Science* 313:976–979
- Pathak MM, Yarov-Yarovsky V, Agarwal G, Roux B, Barth P, Kohout S, Tombola F, Isacoff EY (2007) Closing in on the resting state of the Shaker K⁺ channel. *Neuron* 56:124–140
- Petterson EF, Goddard TD, Huang CC, Couch GS, Greenblatt DM, Meng EC, Ferrin TE (2004) UCSF Chimera—a visualization system for exploratory research and analysis. *J Comput Chem* 25:1605–1612
- Phillips JC, Braun R, Wang W, Gumbart J, Tajkhorshid E, Villa E, Chipot C, Skeel RD, Kalé L, Schulten K (2005) Scalable molecular dynamics with NAMD. *J Comput Chem* 26(16):1781–1802
- Pischalnikova AV, Sokolova OS (2009) The domain and conformational organization in potassium voltage-gated ion channels. *J NeuroImmune Pharmacol* 4:71–82
- Pongs O (2009) Ins and outs of cardiac voltage-gated potassium channels. *Curr Opin Pharmacol* 9:311–315
- Shi G, Trimmer JS (1999) Differential asparagine-linked glycosylation of voltage-gated K⁺ channels in mammalian brain and in transfected cells. *J Membr Biol* 168:265–273
- Sokolova O, Kolmakova-Partensky L, Grigorieff N (2001) Three-dimensional structure of a voltage-gated potassium channel at 2.5 nm resolution. *Structure* 9:215–220
- Sokolova O, Accardi A, Gutierrez D, Lau A, Rigney M, Grigorieff N (2003) Conformational changes in the C terminus of Shaker K⁺ channel bound to the rat Kvβ2-subunit. *Proc Natl Acad Sci U S A* 100:12607–12612
- Sokolova OS, Shaitan KV, Grizel AV, Popinako AV, Karlova MG, Kirpichnikov MP (2012) Three-dimensional structure of human voltage-gated ion channel Kv10.2 studied by electron microscopy of macromolecules and molecular modeling. *Russ J Bioorg Chem* 38(2):152–158
- Suzuki T, Takimoto K (2004) Selective expression of HERG and Kv2 channels influences proliferation of uterine cancer cells. *Int J Oncol* 25:153–159
- Tamkun MM, O'Connell KM, Rolig AS (2007) A cytoskeletal-based perimeter fence selectively corrals a sub-population of cell surface Kv2.1 channels. *J Cell Sci* 120:2413–2423
- Tombola F, Pathak M, Isacoff EY (2006) How does voltage open an ion channel? *Annu Rev Cell Dev Biol* 22:23–52
- Trimmer JS (1991) Immunological identification and characterization of a delayed rectifier K⁺ channel polypeptide in rat brain. *Proc Natl Acad Sci U S A* 88:10764–10768
- Uysal S, Vázquez V, Tereshko V, Esaki K, Fellouse FA, Sidhu SS, Koide S, Perozo E, Kossiakoff A (2009) Crystal structure of full-length KcsA in its closed conformation. *Proc Natl Acad Sci U S A* 106(16): 6644–6649
- van Heel M (1987) Angular reconstitution: a posteriori assignment of projection directions for 3D reconstruction. *Ultramicroscopy* 21: 111–123
- van Heel M, Stoffer-Meilicke M (1985) Characteristic views of the E. coli and B. stearothermophilus 30S ribosomal subunits in the electron microscope. *EMBO J* 4:2389–2395
- van Heel M, Harauz G, Orlova EV, Schmidt R, Scharz M (1996) A new generation of the IMAGIC image processing system. *J Struct Biol* 116(1):17–24
- VanDongen AM, Frech GC, Drewe JA, Joho RH, Brown AM (1990) Alteration and restoration of K⁺ channel function by deletions at the N- and C-termini. *Neuron* 5:433–443
- Vargas E, Bezanilla F, Roux B (2011) In search of a consensus model of the resting state of a voltage-sensing domain. *Neuron* 72(5):713–720
- Wray D (2004) The roles of intracellular regions in the activation of voltage-dependent potassium channels. *Eur Biophys J* 33:194–200
- Wray D (2009) Intracellular regions of potassium channels: Kv2.1 and hKv1.5. *Eur Biophys J* 38:285–292
- Wriggers W (2010) Using Situs for the integration of multi-resolution structures. *Biophys Rev* 2:21–27